Nuclear Instruments and Methods in Physics Research B 348 (2015) 203–208

Contents lists available at ScienceDirect

Nuclear Instruments and Methods in Physics Research B

journal homepage: www.elsevier.com/locate/nimb

Automatic beam focusing in the 2nd generation PBW line at sub-10 nm line resolution

Y. Yao, J.A. van Kan *

Centre for Ion Beam Applications, Department of Physics, National University of Singapore, Singapore 117542, Singapore

ARTICLE INFO

Article history:
Received 25 July 2014
Received in revised form 22 December 2014
Accepted 23 December 2014
Available online 12 January 2015

Keywords:
Proton beam writing
LabVIEW
Automatic focusing
Sub-10 nm

ABSTRACT

Proton beam writing (PBW) has the ability to fabricate high aspect ratio 3D micro/nano-structures with precise edges, smooth and straight side-walls. The newly developed 2nd generation PBW line has a high lens demagnification and is equipped with a superior quality resolution standard, which results in a spatial beam resolution down to 19 nm × 30 nm (van Kan et al., 2012). Fine lithographic hydrogen silsesquioxane (HSQ) patterns featuring 19 nm line width and 60 nm spacing have been fabricated using the 2nd generation PBW line (Yao et al., 2014). In those experiments, beam focusing was done by manually adjusting the currents of the magnetic quadrupole lens power supplies to achieve a small beam spot size. Here we present an automatic focusing program which can focus a 2 MeV proton beam down to 9.3 nm × 32 nm in less than 10 min.

1. Introduction

Proton beam writing (PBW) is a direct-write lithography technique, which uses a focused MeV proton beam to fabricate micro or nano patterns. Compared with other lithography techniques such as electron beam lithography, UV lithography or focused ion beam (FIB), PBW has its unique advantages. First, in proton beam writing, the protons mainly interact with the electrons. Because of the large difference in mass between proton and electron ($m_p/m_e \approx 1800$), the energy transfer in every collision is very small and hundreds of thousands of collisions will occur before a proton has lost all its energy. Therefore a proton beam penetrating a material will have a large range and almost straight path except at the end of range where nuclear scattering becomes more pronounced. It offers a method to fabricate high aspect ratio structures with smooth and straight side walls [3]. Secondly, since the penetration depth depends on the beam energy, by changing the beam energy, multilevel structures can be fabricated [4]. Moreover, PBW can serve as a versatile tool for rapid prototyping using a variety of materials without the need for expensive masks. Owing to these properties, PBW has been used in many areas like photonics [5,6], micro or nano fluidics [7,8], nano imprinting [9], silicon machining [10,11] and masks for X-ray lithography [12].

At the Centre for Ion Beam applications (CIBA), in the Department of Physics, National University of Singapore, there exist two proton beam writing lines [13,14]. The first generation PBW line has the ability to focus proton beam down to 35 × 75 nm^2 [15]. 100 nm grooves have been fabricated in positive PMMA resist [2]. Sub-100 nm details have only been obtained in negative resists SU-8 and HSQ, featuring 60 and 22 nm wide lines respectively [4,16]. The newly developed 2nd generation PBW line has the capability of high demagnification, which can give a beam resolution down to 19 × 30 nm^2 and single line scan with beam width of 12.6 nm [1]. HSQ lines down to 19 nm in width and 100 nm tall have been demonstrated, which are the smallest features ever written in PBW [17].

Although PBW has seen significant progress in the last 2 decades, it is still relatively immature compared with electron beam lithography. There are many issues waiting to be solved or optimized. One of the issues is beam focusing. Because of the high energy and high mass of the ions, magnetic quadrupole lenses are used to focus down the beam [18]. In our system, a spaced Oxford lens configuration is used. Beam focusing is normally achieved by manually adjusting the currents of magnetic quadrupole lenses and monitoring the beam profile. The beam size is gauged by measuring the distance between two points where the signal intensity is 88% and 12% of the maximum [19,20]. This focusing process is time consuming (1–2 h) and difficult to accurately determine the beam spot. An automatic focusing system based on C++ had been developed and a sub-micrometer beam spot of approximately (700 × 600 nm^2) was achieved in the first generation proton beam writing system [21]. However, because of the different data acquisition system, this program is not compatible with the 2nd

* Corresponding author.
E-mail address: phyjavk@nus.edu.sg (J.A. van Kan).

http://dx.doi.org/10.1016/j.nimb.2014.12.066
0168-583X/

generation PBW system. Here we demonstrate higher beam resolution by automatic focusing compared to manual focusing and earlier automatic focusing [21]. This automatic focusing program can easily focus a proton beam down to 9.3 nm × 32 nm in less than 10 min.

2. Hardware

The proton beam writing system follows the normal layout of ion beam microprobe. Proton beam transmits through a set of object and collimator slits and is then focused on the imaging plane by means of a series of strong magnetic quadrupole lenses. Although a magnetic quadrupole lens has very strong focusing action, it can only focus the beam in one direction and defocus the beam in another direction. Therefore it requires a minimum of two lenses of opposite polarity to focus beam down to a small spot [18]. To achieve high demagnification, the quadrupole lens system is operated in a spaced Oxford triplet configuration, where the first two lenses are coupled and excite equally [1]. Currently, by choosing a 30 mm working distance, the system has a demagnification up to 857 × 130 in *X* and *Y*, respectively [10]. The quadrupole lenses are powered by two Bruker power supplies, which can provide a maximum current of 120 A with a stability of 2 ppm. The power supplies are equipped with Ethernet interface, allowing for remote control.

The data acquisition, beam control and scanning system utilizes National Instruments M-Series PCI/PXI 6259 DAQ card. This card has an additional feature, which allows a *buffered counter acquisition* that makes use of the counter's gate input. With this mode, the data acquisition system can handle fast scan speed imaging (100 kHz pixel update time). More of the card information and imaging algorithm can be found elsewhere [22]. To scan the beam across a sample, an electrostatic scanning system is installed. The electrostatic scanning requires high voltages and high (±4 kV Trek, 609E6) or low voltage (±220 V Techron) amplifiers are used to appropriately amplify the outputs from the DAQ card. Two orthogonal scanning plates are placed before the lens system to scan the *X* and *Y* direction respectively [1]. One important feature of the scanning system is that the output voltage from the card has a range from −10 to 10 V with an absolute accuracy of about 2 mV. This accuracy error causes a fluctuation of beam position, which further influences the beam size measurement. In order to make sure that the beam size measurement error is less than 1 nm, when the output voltage is from −10 to 10 V, the maximum scan size should be no larger than 5 μm.

In most of ion beam microprobe experiments, a commercial resolution standard is used to focus down the beam. However, when the beam size is sub-micron, this commercial resolution standard is not sufficient to accurately determine the beam spot size. Since PBW has the ability to fabricate high aspect ratio 3D micro/nanostructure with precise edges, smooth and straight side-walls, it is an ideal tool to produce high quality resolution standards. Early resolution standards produced using PBW had a thickness of 10 μm and a beam spot size of 280 nm × 420 nm^2 was demonstrated [23]. Later, a 2 μm thick free standing nickel resolution standard with a sidewall projection of 14 nm was proven to be more useful for focusing a beam to sub-30 nm [9]. Recently, an even higher quality free standing Ni resolution standard was fabricated and equipped in the 2nd generation proton beam line [24]. This new resolution standard has an orthogonality of 90.0° ± 0.1°, and a side-wall slope projection of less than 6 nm. It has been used successfully in the process of focusing H_2^+ beam to 14 × 39 nm^2.

A STIM signal is used for imaging since it does not require prolonged time to collect sufficient statistics. A PIN diode detector positioned behind the sample on a movable arm provides flexible count rate and imaging modes. When the beam count rate is higher than 20 kHz, the scattered beam is analyzed using off-axis STIM mode to protect the detector. To achieve ultimate small spot sizes, the beam current is reduced to a few tens of thousands of protons per second and the direct un-scattered beam is analyzed in the on-axis STIM mode.

3. Focusing

An automatic beam focusing system requires rapid monitoring of the variation of the full width at half maximum (FWHM) of the beam spot in both *X* and *Y* directions, in response to the changes of the magnetic quadrupole lens currents. In our approach, the FWHM is gauged by monitoring the line scan resulting from the beam being scanned over a sharp edge. The corresponding STIM signal contains the required information about the beam profile and the beam size is obtained by de-convoluting the beam profile. Since the proton beam has a Gaussian distribution, the beam profile in one dimension can be expressed as

$$F(x) = a\left[1 + \mathrm{erf}\left(\frac{2\sqrt{ln2}}{f}(b - x)\right)\right]$$

where *f* is the FWHM of the beam spot in the scan direction, *a* is a constant and scales the counts and *b* is the position of the edge along the scan. Then the mathematical fitting of the above function to the line scan data is achieved by means of the non-linear Levenberg–Marquardt method [25].

LabVIEW 2011 [26] is the programming environment chosen for automatic focusing. A key feature of LabVIEW is extensive support for accessing instrument hardware. Furthermore, because it provides a variety of driver interfaces, people with limited coding experience can write programs and do tests in a short time.

When the program images the resolution standard, the user can easily draw a vertical and horizontal line which cross over the sharp edges of the resolution standard. Since beam size in *X* direction is more related to the current of the last lens and beam size in *Y* direction is more related to the current of the first two lenses when the system is near to optimum focus, the best focus in one direction is achieved by changing the relevant lens current.

A typical starting current in the two power supplies (A and B) can be chosen from a data base or can be found through focusing by hand, employing the feedback from the beam induced fluorescence in a quartz sample. Then two current step sizes are chosen (A′, B′) for each lens power supply. First the program will change the current in one power supply in five steps from A − 2A′ to A + 2A′ and the current corresponding to the smallest beam size is selected. Next the program will change the current in the other lens power supply following the same procedure. Then the current step size is reduced to half and the whole optimization process is repeated several times to get the final results. Since the initial current is very close to the optimized current and the step size is relatively small compared with starting current, the hysteresis effect is not noticeable.

4. Experiments and results

A 2 MeV proton beam passes through object slits with an opening of 7 × 3 μm^2 and is further collimated by aperture slits of 30 × 30 μm^2. The imaging system is fixed at an update time of 20 μs per pixel with 256 × 256 pixel resolution and a scan size of 32.5 × 32.5 μm^2. A pin diode is positioned in off-axis STIM mode which gives a count rate of ~13 kHz. After imaging the resolution standard, two lines with 256 pixels, which cross the resolution standard edges, are drawn on the image to measure the beam sport size. The total line counts for every scan are fixed at 4 K, which

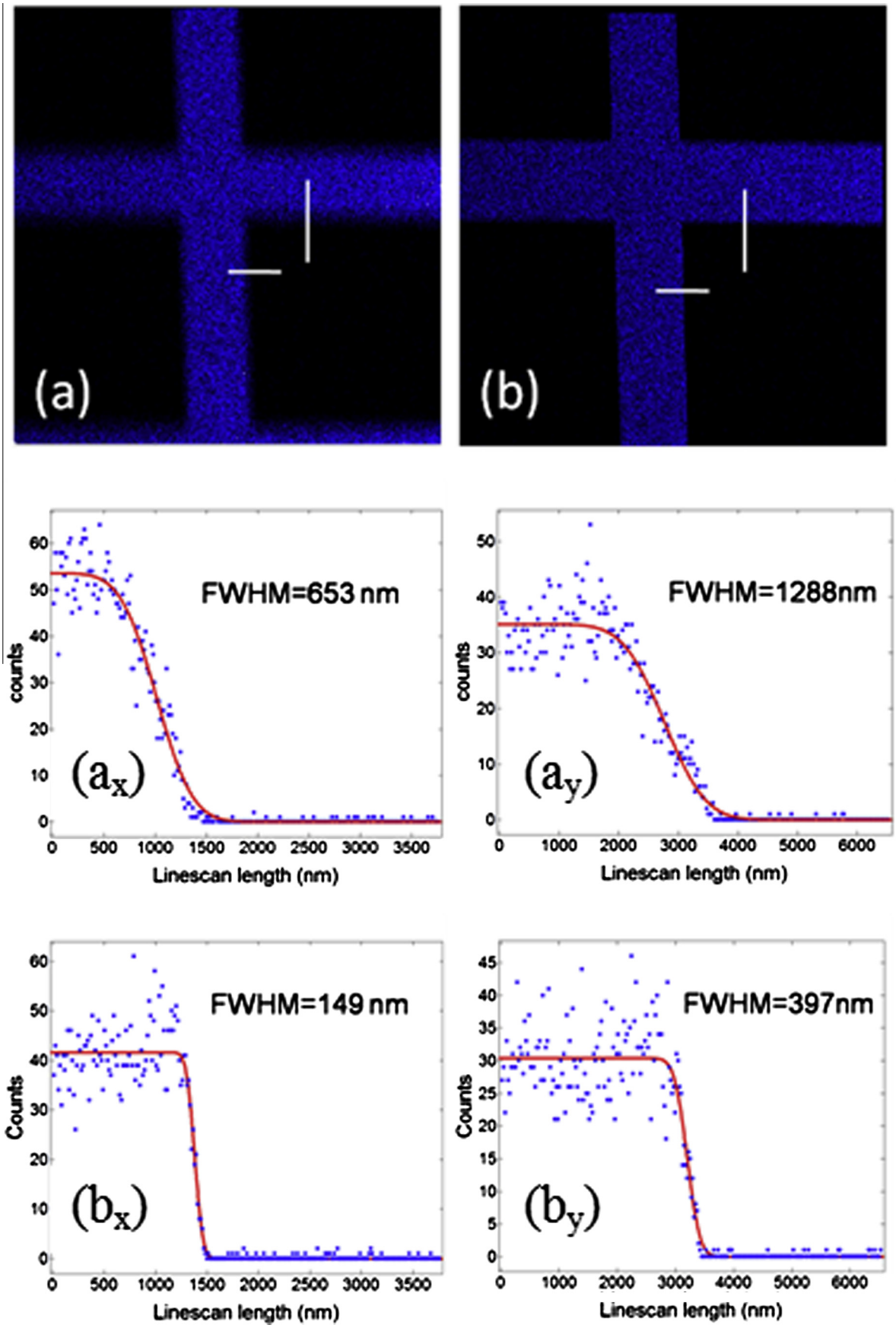

Fig. 1. Off-axis scanning transmission ion microscopy images of the Ni resolution standard (a and b) and the extracted beam profiles (a_x, a_y, b_x and b_y). The STIM images are taken before focusing (a) and after first time automatic focusing (b). Both of the images (a and b) have a scan area of 32.5 × 32.5 μm^2. The beam profiles are extracted from the regions as shown in figure (a and b) with a white marker line. For example, the figures (a_x) and (a_y) are extracted from figure (a) in *X* and *Y* direction respectively.

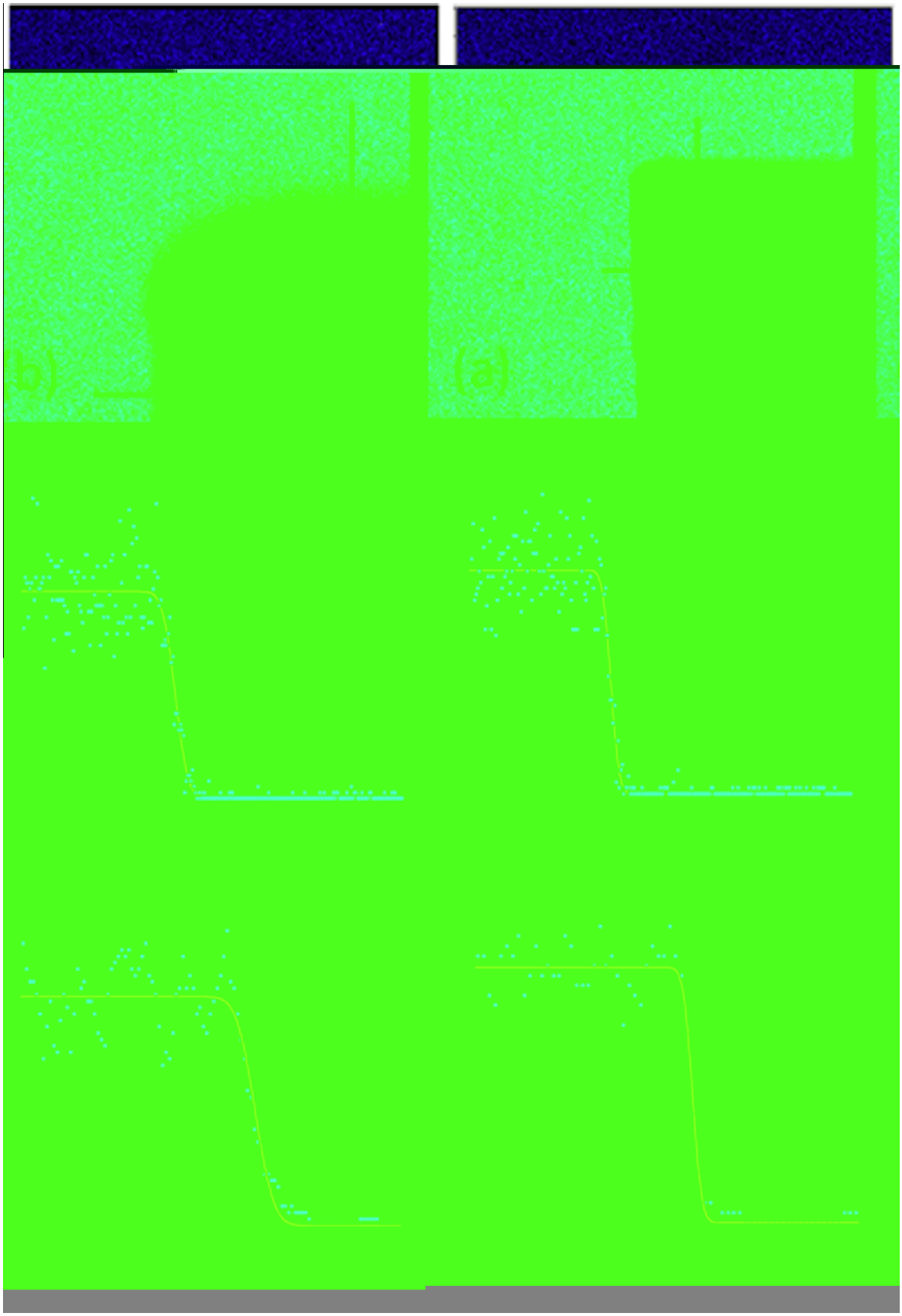

Fig. 2. Off-axis scanning transmission ion microscopy images of the Ni resolution standard (a and b) and the extracted beam profiles (a_x, a_y, b_x and b_y). The STIM images are taken after second time focusing (a) and final imaging (b). The images (a and b) have a scan size of $4 \times 4\ \mu m^2$ and $800 \times 800\ nm^2$ respectively. The figures (a_x) and (a_y) are extracted from figure (a) with white marker lines in *X* and *Y* direction respectively. The figures (b_x) and (b_y) are extracted from figure (b) with white marker lines in *X* and *Y* direction respectively.

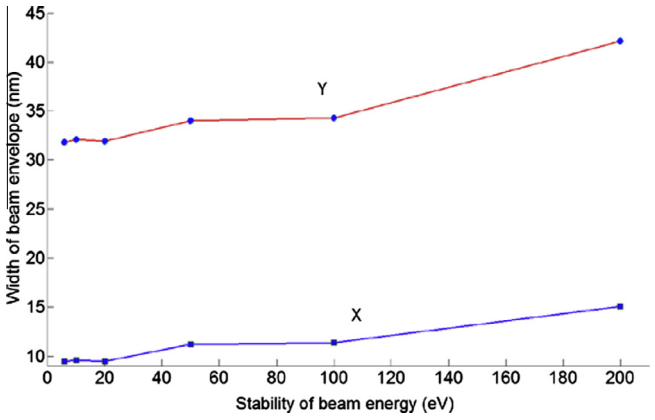

Fig. 3. Simulation of the beam width on the imaging plane as a function of beam energy stability. This simulation is obtained by software PBO Lab. The initial beam is 2 MeV proton. The object slits and collimator slits have openings of 8×4 and 30×30 μm^2 respectively. The beam has a width of 9.5×31.8 nm^2.

requires tens of frames to be scanned for every beam size measurement. As shown in Fig. 1a, a_x and a_y, before focusing, the beam has a resolution of about 653×1288 nm^2. Then, the beam is focused with the LabVIEW program by adjusting the lens currents. This process normally takes 2–5 min. After focusing, the fitting curve indicates a beam spot size of about 149×397 nm^2 (Fig. 1b, b_x and b_y). Considering the noise level of the NI card as mentioned above, the beam scan size is then set to 4×4 μm^2 by reducing the amplification to further focus down the beam. The iteration continues until the step size is smaller than the setting current error level (0.001 A). After the second time beam focusing, the STIM image is shown in Fig. 2a, which indicates a beam spot size of 14×30 nm^2 (see Fig. 2a_x and a_y). Finally, in order to double check the beam spot size, an area of 800×800 nm^2 with 256×256 pixel resolution is scanned for more than 20 times. The fitting data are directly extracted from the image. Since the count is at a low level, 4 adjacent and 6 adjacent lines are added in *X* and *Y* direction respectively to get enough statistics. As shown in Fig. 2b, b_x, and b_y, a beam resolution of 9.3 nm $\times$ 32 nm is achieved.

4.1. Beam stability

The stability of the beam energy and the lens power supplies is very important to maintain the same beam size for a long time. The 3.5 MV high energy Singletron accelerator in CIBA has a beam energy stability of about 20 eV [27]. Here we simulate the width of the beam envelope on the image plane as a function of the beam energy stability (Fig. 3). This simulation is obtained by software Particle Beam Optics Laboratory 3.0 (PBO Lab) [28]. The initial beam is 2 MeV proton with a stability of 6 eV. The object slits and collimator slits have openings of 8×4 and 30×30 μm^2 respectively. The working distance is set to 30 mm. The simulation result shows that if the beam energy stability is less than 20 eV, the energy fluctuation almost has no effect on the width of the beam envelope. Further the width of the beam envelope is 9.5×31.8 nm^2, which is a little larger than the simple calculation result of 9.3 nm (8000/857) $\times$ 30.8 nm (4000/130) (not taking any aberrations into account). The small difference is mainly due to intrinsic and parasitic aberrations of this system. Now, considering the lens power supply stability, the magnetic field of the quadrupole lens is proportional to the root of the beam energy. For a 2 MeV beam, the lens power supply stability of 2 ppm is equivalent to a beam energy variation of 8 eV, which is well below the required energy stability of 20 eV.

5. Summary and outlook

We have successfully demonstrated the possibility of automatic focusing in the 2nd generation proton beam writing system. LabVIEW is chosen as the programming environment. A final beam spot size of 9.3×32 nm^2 is achieved. The whole focusing process takes less than 10 min. It reduces the focusing time by one order compared to manual focusing, achieves significantly better focus and is more convenient for the users.

In this experiment, the system had a lens demagnification of 857×130 and the object slits had an opening of 7×3 μm^2. Within the accuracy of the object opening (1 μm), this final achieved beam spot size (9.3 nm $\times$ 32 nm) exactly matches the simulation result (9.5 nm $\times$ 31.8 nm). Thermal fluctuation in the lens system is the main issue which enlarges the beam size in *Y* direction. To reduce this drift, a vortex fan has been used to stabilize the lens temperature within ±0.1 °C. We are also looking for a better ways to reduce the thermal fluctuation. Furthermore, the major limitation in achieving better resolution is the lack of a high brightness ion source, which is currently under development at CIBA in collaboration with Delft University [29,30].

Acknowledgments

The authors acknowledge the financial support rendered by the U.S. Air Force, Japan office.

References

[1] J.A. van Kan, P. Malar, A. Baysic de Vera, Rev. Sci. Instrum. 83 (2012) 02B902.
[2] Y. Yao, P. Santhana Raman, J.A. van Kan, Microsyst. Technol. 20 (2014) 2065–2069.
[3] F. Watt, M.B.H. Breese, A.A. Bettiol, J.A. van Kan, Mater. Today 10 (2007) 20–29.
[4] J.A. van Kan, A.A. Bettiol, K. Ansari, E.J. Teo, T.C. Sum, F. Watt, Int. J. Nanotechnol. 1 (2004) 464–479.
[5] T.C. Sum, A.A. Bettiol, H.L. Seng, I. Rajta, J.A. van Kan, F. Watt, Nucl. Instr. Meth. Phys. Res., Sect. B 210 (2003) 266–271.
[6] F. Chen, Laser Photonics Rev. 6 (2012) 622–640.
[7] J.A. van Kan, C. Zhang, P. Perumal Malar, J.R.C. van der Maarel, in: Biomicrofluidics 6 (2012) 036502.
[8] H.J. Whitlow, L.P. Wang, L. Gilbert, Transport of water and particles in microfluidics devices lithographically fabricated using proton beam writing (PBW), in: S. Teo, A.Q. Liu, H. Li, B. Tarik (Eds.), Nems/Mems Technology and Devices, Trans Tech Publications Ltd., Stafa-Zurich, 2009, pp. 129–132.
[9] K. Ansari, P.G. Shao, J.A. van Kan, A.A. Bettiol, F. Watt, Nucl. Instr. Meth. Phys. Res., Sect. B 231 (2005) 407–412.
[10] Z. Dang, A. Banas, S. Azimi, J. Song, M. Breese, Y. Yao, S.P. Turaga, G. Recio-Sánchez, A. Bettiol, J.A. van Kan, Appl. Phys. A 112 (2013) 517–523.
[11] I. Rajta, S.Z. Szilasi, P. Furjes, Z. Fekete, C. Ducso, in: Nucl. Instr. Meth. Phys. Res. Sect., B 267 (2009) 2292–2295.
[12] W. Yue, Sher-Yi Chiam, Y. Ren, J.A. van Kan, T. Osipowicz, L. Jian, H.O. Moser, F. Watt, J. Micromech. Microeng. 18 (2008) 085010.
[13] J.A. van Kan, P. Malar, A.B. de Vera, X. Chen, A.A. Bettiol, F. Watt, Nucl. Instr. Meth. Phys. Res., Sect. A 645 (2011) 113–115.
[14] F. Watt, J.A. van Kan, I. Rajta, A.A. Bettiol, T.F. Choo, M.B.H. Breese, T. Osipowicz, Nucl. Instr. Meth. Phys. Res., Sect. B 210 (2003) 14–20.
[15] J. A. van Kan, A. Bettiol, F. Watt, MRS Proceedings, Cambridge Univ Press 2003, pp. T2. 1.
[16] J.A. van Kan, A.A. Bettiol, F. Watt, Nano Lett. 6 (2006) 579–582.
[17] Y. Wang, P. Malar, J.A. van Kan, Microsyst. Technol. 20 (2014) 2079–2088.
[18] G.W. Grime, F. Watt, Beam Optics of Quadrupole Probe-forming Systems, Adam Hilger Limited, 1984.
[19] A.A. Bettiol, C. Udalagama, J.A. van Kan, F. Watt, Nucl. Instr. Meth. Phys. Res., Sect. B 231 (2005) 400–406.
[20] F. Watt, X. Chen, A.B.D. Vera, C.N. Udalagama, M. Ren, J.A. van Kan, A.A. Bettiol, Nucl. Instr. Meth. Phys. Res., Sect. B 269 (2011) 2168–2174.
[21] C.N.B. Udalagama, A.A. Bettiol, J.A. van Kan, E.J. Teo, M.B.H. Breese, T. Osipowicz, F. Watt, Nucl. Instr. Meth. Phys. Res., Sect. B 231 (2005) 389–393.
[22] C. Udalagama, A.A. Bettiol, F. Watt, J. Microsc. 238 (2010) 185–188.
[23] F. Watt, I. Rajta, J.A. van Kan, A.A. Bettiol, T. Osipowicz, Nucl. Instr. Meth. Phys. Res., Sect. B 190 (2002) 306–311.
[24] Y. Yao, M.W. van Mourik, P. Santhana Raman, J.A. van Kan, Nucl. Instr. Meth. Phys. Res., Sect. B 306 (2013) 265–270.
[25] J. Moré, The Levenberg–Marquardt algorithm: implementation and theory, in: G.A. Watson (Ed.), Numerical Analysis, Springer, Berlin Heidelberg, 1978, pp. 105–116.
[26] <http://www.ni.com/labview/release-archive/2011/>.

[27] D. Mous, R. Haitsma, T. Butz, R.-H. Flagmeyer, D. Lehmann, J. Vogt, Nucl. Instr. Meth. Phys. Res., Sect. B 130 (1997) 31–36.
[28] <http://www.ghga.com/accelsoft/pbolab.html>.
[29] D.S. Jun, V.G. Kutchoukov, P. Kruit, J. Vac. Sci. Technol., B 29 (2011) 06F603.
[30] N. Liu, P. Santhana Raman, X. Xu, H. M. Tan, A. Khursheed, J. A. van Kan, this proceedings.